UC Irvine
UC Irvine Previously Published Works

Title
BES upgrade

Permalink

Journal

ISSN

Authors
Bai, JZ
Bao, HC
Blum, I
et al.

Publication Date

DOI

Copyright Information

Peer reviewed

The BES upgrade

J.Z. Bai[a], H.C. Bao[a], I. Blum[b], Z.W. Chai[a], G.P. Chen[a], H.F. Chen[c], J. Chen[d],
J.C. Chen[a], Y. Chen[a], Y.B. Chen[a], Y.Q. Chen[a], B.S. Cheng[a], X.M. Chu[a], X.Z. Cui[a],
H.L. Ding[a], W.Y. Ding[a], L.Y. Dong[a], Y.Y. Du[a], Z.Z. Du[a], W. Dunwoodie[e], J. Fang[a],
W.Z. Fang[a], C.S. Gao[a], M.L. Gao[a], S.Q. Gao[a], P. Gratton[b], J.H. Gu[a], S.D. Gu[a],
W.X. Gu[a], Y.N. Guo[a], H.G. Han[a], S.W. Han[a], F.A. Harris[f], Y. Han[a], J. He[a], M. He[g],
Y.K. Heng[a], D.G. Hitlin[h], G.Y. Hu[a], H.B. Hu[a], H.M. Hu[a], J.L. Hu[a], Q.H. Hu[a],
T. Hu[a], X.Q. Hu[a], G.S. Huang[a], J.D. Huang[a], Y.Z. Huang[a], J.M. Izen[b], C.H. Jiang[a],
Y.Y. Jiang[a], Y. Jin[a], B.D. Jones[b], X. Ju[a], Z.J. Ke[a], M.H. Kelsey[k], B.K. Kim[b],
D. Kong[f], Y.F. Lai[a], P.F. Lang[a], A. Lankford[i], C.G. Li[a], F. Li[a], H.B. Li[a], J. Li[a],
P.Q. Li[a], Q. Li[g], R.B. Li[a], W. Li[a], W.D. Li[a], W.G. Li[a], W.H. Li[a], X.H. Li[a], X.N. Li[a],
H.M. Liu[a], J. Liu[a], J.H. Liu[a], Jun Liu[a], Q. Liu[a], Q.J. Liu[a], R.G. Liu[a], Y. Liu[a],
Z.X. Liu[a], J.S. Lou[a], X.C. Lou[b], B. Lowery[b], H.Y. Lu[a], J.G. Lu[a], H. Luo[a], S.Q. Luo[a],
X.L. Luo[a], E.C. Ma[a], J.M. Ma[a], R. Malchow[d,*], M. Mandelkern[i], H.S. Mao[a],
Z.P. Mao[a], X.C. Meng[a], X.H. Mo[a], L.G. Mu[a], H.L. Ni[a], J. Nie[a], S.L. Olsen[f],
J. Oyang[h], D. Paluselli[f], L.J. Pan[f], J. Panetta[h], F. Porter[h], N.D. Qi[a], X.R. Qi[a],
C.D. Qian[j], J.F. Qiu[a], Y.H. Qu[a], Y.K. Que[a], G. Rong[a], M. Schernau[i], B. Schmid[i],
J. Schultz[i], Y.Y. Shao[a], B.W. Shen[a], D.L. Shen[a], H. Shen[a], X.Y. Shen[a], H.Y. Sheng[a],
H.Z. Shi[a], X.F. Song[a], J. Standifird[b], D. Stoker[i], F. Sun[a], H.S. Sun[a], S.J. Sun[a],
Y. Sun[a], Y.Z. Sun[a], Y.P. Tan[a], S.Q. Tang[a], W. Toki[d], G.L. Tong[a], G.S. Varner[f],
Z.R. Wan[a], F. Wang[a], J.F. Wang[a], L. Wang[a], L.S. Wang[a], L.Z. Wang[a], Meng Wang[a],
P. Wang[a], P.L. Wang[a], S.M. Wang[a], T.J. Wang[a,*], Y.Y. Wang[a], M. Weaver[h],
C.L. Wei[a], D.M. Xi[a], X.M. Xia[a], X. Xiao[a], P.P. Xie[a], Q. Xie[a], Y. Xie[a], Y.H. Xie[a],
W.J. Xiong[a], C.C. Xu[a], Z.Q. Xu[a], S.T. Xu[a], J. Yan[a], W.G. Yan[a], B. Yang[a],
C.M. Yang[a], C.S. Yang[a], C.Y. Yang[a], D.J. Yang[a], G.A. Yang[a], H.X. Yang[a], J. Yang[a],
X.F. Yang[a], W. Yang[d], W.L. Yao[a], M.H. Ye[a], C.S. Yu[a], C.X. Yu[a], Y.H. Yu[k], Z.Q. Yu[a],
C.Z. Yuan[a], Y. Yuan[a], B.Y. Zhang[a], C.C. Zhang[a], D.H. Zhang[a], Dehong Zhan[a],
H.L. Zhang[a], J. Zhang[a], J.W. Zhang[a], Lin. Zhang[a], L. Zhang[a], P. Zhang[a],

*Corresponding address. Department of Physics and Astronomy, Georgia State University, 29 Peachtree Center Avenue, Atlanta GA 30303-3083, USA. Tel.: +1-404-651-2279; fax: +1-404-651-1427.

E-mail address: phyrlmx@panther.gsu.edu (R. Malchow).
✠ Deceased

Q.J. Zhang[a], S.Q. Zhang[a], Y. Zhang[g], Y.Y. Zhang[a], D.X. Zhao[a], H.W. Zhao[a],
J.W. Zhao[a], M. Zhao[a], W.R. Zhao[a], Z.G. Zhao[a], J.P. Zheng[a], L.S. Zheng[a],
S.C. Zheng[a], Z.P. Zheng[a], C.C. Zhong[a], B.Q. Zhou[a], G.P. Zho[a], H.S. Zhou[a],
L. Zhou[a], X.F. Zhou[a], K.J. Zhu[a], Q.M. Zhu[a], Y.C. Zhu[a], Y.S. Zhu[a], B.A. Zhuang[a]

[a]*Institute of High Energy Physics, Beijing 100039, People's Republic of China*
[b]*University of Texas at Dallas, Richardson, TX 75083-0688, USA*
[c]*University of Science and Technology of China, Hefei 230026, People's Republic of China*
[d]*Colorado State University, Fort Collins, CO 80523, USA*
[e]*Stanford Linear Accelerator Center, Stanford, CA 94309, USA*
[f]*University of Hawaii, Honolulu, HI 96822, USA*
[g]*Shandong University, Jinan 250100, People's Republic of China*
[h]*California Institute of Technology, Pasadena, CA 91125, USA*
[i]*University of California at Irvine, Irvine, CA 92717, USA*
[j]*Shanghai Jiaotong University, Shanghai 200030, People's Republic of China*
[k]*Hangzhou University, Hangzhou 310028, People's Republic of China*

Abstract

The Beijing Spectrometer (BES) detector is a general purpose solenoid detector at the Beijing Electron Positron Collider (BEPC) in Beijing, China, that has collected large numbers of J/ψ, ψ', D$_s$, D and τ events. In this paper, we describe the recent upgrade of the initial BES detector (BESI) to the improved BESII detector. © 2001 Elsevier Science B.V. All rights reserved.

1. Introduction

The Beijing Spectrometer (BES) occupies the sole interaction point at the Beijing Electron Positron Collider (BEPC). BES is a conventional cylindrical magnetic detector. The initial configuration of the detector, BESI, is described in detail in Ref. [1]. It consists of the following subsystems: central drift chamber (CDC), main drift chamber (MDC), time-of-flight counters (TOF) (barrel and endcap), electromagnetic shower counter (SC), muon chamber, luminosity monitor (LUM), solenoid magnet, trigger, and online data acquisition system (DAQ).

BESI has collected about 9 million J/ψ events [2], 3.8 million ψ' events [3], and 22.3 pb^{-1} of D and D$_s$ events [4]. The measurement of the τ lepton mass at production threshold was performed at a machine luminosity of 5×10^{30} cm^{-2} s^{-1} [5].

After running the BESI detector for five years, aging effects were seen. The pulse height of the MDC dropped, the dark current of MDC layers 8–10 increased above normal values for some wires, the attenuation length of the scintillation counters in the TOF decreased, and the TOF time resolution degraded from 330 to 375 ps.

To increase the luminosity of BEPC and improve the performance of BES, upgrades of both were done from 1993 to 1997. This paper emphasizes the description of new or upgraded main subsystems and the final performance of BESII. When necessary to avoid ambiguity, the older systems are referred to as version I (e.g. MDCI), while new and upgraded systems are referred to as version II (e.g. MDCII). The improvements to BEPC are described in Ref. [6].

To improve the performance of BES and suppress background, we have built a new drift
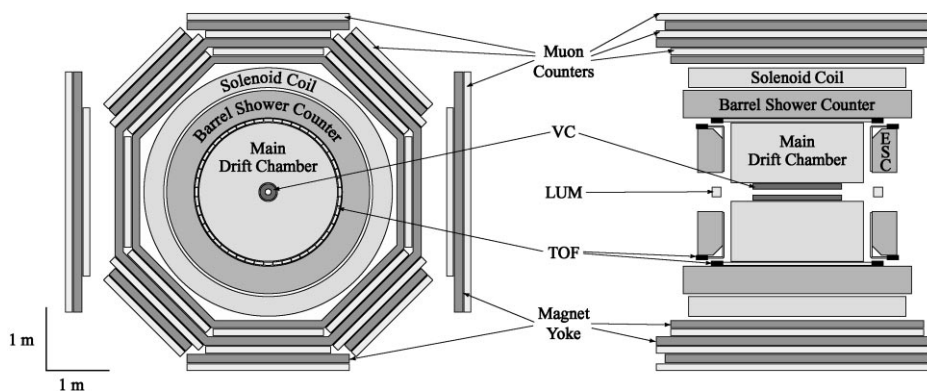
Fig. 1. End view (left) and side view (right) of the BESII detector.

chamber (MDCII), new time-of-flight counter (TOFII), a new luminosity monitor compatible with a low-β lattice (LUMII), and rebuilt the vertex chamber (VC) from MarkIII to replace the old CDC. The DAQ system and trigger readout were upgraded to increase speed and decrease deadtime. The offline software was converted from VAX/VMS to HP/UNIX, and new tracking software and simulation codes for the MDCII and VC were written. Other systems such as the shower counter, gas system, and cooling system were carefully repaired or modified. As of 1997, BES has been operating in the upgraded BESII configuration (as shown in Fig. 1). Long-term operation has shown that the upgrades have been successful.

2. New main drift chamber (MDCII)

The drift chamber is the main tracking detector of BES. Its main functions are to determine trajectories and measure the energy loss of charged particles and provide information for the trigger system.

Both MDCI and MDCII are 10 layer, open-cell geometry drift chambers. The design improvements for MDCII include a smaller drift cell size, a more symmetric cell arrangement, better field shaping, and improved feedthrough design. MDCII has 804 drift cells and 3216 sense wires, as compared to MDCI which had only 702 cells and 2808 sense

Table 1
Comparison of MDCI and MDCII characteristics

	MDCI	MDCII
Cells	702	804
Total wires	19 380	22 936
Sense wires	2808	3216
Symmetry	2-fold	4-fold
Feedthrough	2 parts	1 part
Layer 10 design voltage	4.25 kV	3.8 kV

wires. In addition to improving spatial and momentum resolution, the smaller drift distance allows MDCII to be operated at a lower voltage while maintaining drift velocity saturation. For example, the design voltage of layer 10 has been lowered to 3800 V in MDCII, compared with 4250 V in MDCI. Table 1 summarizes the differences between MDCII and MDCI.

From a tracking and triggering point of view, a drift chamber should have n-fold symmetry to simplify the trigger design and off-line track reconstruction. From a detection point of view, the relative position of the cells from layer to layer should be randomized in order to obtain good tracking resolution for charged tracks with different momenta. In the design of MDCII, the whole chamber has at least four-fold symmetry, with the inner four layers having eight-fold symmetry. In each quarter of the chamber the cell pattern from layer to layer is random.

The gains of layers one and 10 are different from other layers due to their positions near the inner and outer cylinders of the chamber. Additional field shaping wires are included in these layers to compensate for this effect.

The function of the feedthroughs in the MDC is to position the wires accurately, electrically insulate the wires from the endplates, bring high voltage into the chamber, and allow tracking signals to be brought out through solder pins inserted into the feedthroughs. The feedthroughs of MDCI were produced form Delrin in two pieces which were then glued together. The small gap between the two parts, about halfway along the axis of the feed through, was filled with epoxy. During operation of MDCI, the epoxy joints broke down, producing a large leakage current after long-term operation. To remedy this, the feedthroughs for MDCII were made as a single piece of Delrin, 5.8 cm long. They were injection molded with a tolerance on the location of the wire-positioning hole of 50 μm.

Unfortunately, leakage current and noise increased rapidly after about two months of running MDCII. Cracks appeared on the surface of the feedthroughs and several holes developed through the insulator. Review of feedthrough production procedures revealed that the virgin Delrin had been mishandled when the feedthroughs were injection molded. The mold cavity temperature was too low, producing poorly crystallized Delrin with a stressed skin. The stress was relieved by the formation of small cracks in the surface. When voltage was applied, microdischarging in these cracks eroded the Delrin, resulting in the observed electronic noise, leakage current, and eventual punctures. Because the chamber was operated with high voltage on the field wires and the sense wires at ground potential, high leakage currents affected only the field wires. However, microdischarging in the field wire feedthroughs was capacitively coupled to the sense wires, resulting in high noise levels.

This problematic leakage current and noise were found to depend strongly on the voltage on the feedthroughs. To decrease the noise to a satisfactory level, the voltage on the field wires would have to be decreased from 3800 to 2000 V. Thus, a split voltage scheme was adopted: the maximum voltage on the signal wires was set at $+2000$ V, while the voltage of field wires was set at -1800 V. The Chamber has been successfully operated in this configuration [7].

3. New time-of-flight counter (TOFII)

The barrel part of the time-of-flight counter consists of 48 scintillation counters. The goal of the upgrade of the TOF was to improve the performance without a large change in the physical configuration and readout electronics.

There are many factors which affect time resolution, including the bunch length, fluctuation of the start signal, electronics, and signal transmission in the cables. However, the main factors which affect the inherent time resolution of the TOF system are the three main components of scintillation counter: the scintillator material, the light pipe, and the phototubes. The best resolution is obtained using a scintillator with a short decay time, a short light guide, and a fast photomultiplier tube (PMT) suitable for a high magnetic field environment.

The structure of the barrel scintillation counters in TOFII is the same as that of TOFI: bars of scintillator are arranged in a cylinder just outside the MDC (see Fig. 1). Each bar is connected to two PMTs, one on each end of the bar. The scintallator bars are 284 cm long, 15.6 cm wide and 5 cm thick. The scintillator used for TOFII was BC-408, which has a fluorescence decay time of 2.1 ns and an attenuation length of 4.4 m. In comparison, TOFI used the scintillator NE110 with a decay time of 2.3 ns and an attenuation length of 2.5 m. Fine mesh R2490-05 (FM) PMT's were used in TOFII. Table 2 shows the differences between TOFI and TOFII. The time resolution measured with cosmic rays is better than 150 ps for one counter.

Table 2
Comparison of TOFI and TOFII characteristics

	TOFI	TOFII
Scintillator	NE110	BC-408
Phototubes	XP2020	R2409-05
Light guide length	112 cm	16 cm
Attenuation length	2.5 m	4.4 m

4. Vertex chamber (VC)

The vertex chamber (VC), which was obtained from the decommissioned MarkIII detector at SLAC, was rebuilt and installed in BES. The VC is built around a 9.8 cm diameter beryllium beampipe (1.2 mm thick), which replaced the BESI aluminum beampipe (2.0 mm thick). There are 12 layers of straws in the chamber; layers 1–4 and 9–12 are axial, while layers 5–8 are stereo, making an angle of about 3° with respect to the beam axis. Layers 1–8 have 40 straws each, and layers 9–12 have 80 straws each, for a total of 640 straws in the chamber. The straws are made of two layers of 25 μm thick mylar wrapped in a helix. The inner mylar layer has a thin layer of aluminum evaporated on the inner surface. All of the straws are 8 mm in diameter and are strung with 50 μm gold-plated tungsten wire. The layers are staggered in ϕ by one-quarter cell, so there will be a minimum of two hits in the inner four axial layers and two hits in the outer four axial layers for each straight track coming from the interaction point. The straws are held between two inner endplates 83 cm apart. The gas volume is defined by the beampipe at the inner radius (4.9 cm), a carbon fiber/epoxy composite shell at the outer radius (13.5 cm), and high-pressure outer endplates at each end (130 cm apart). Fig. 2 shows the arrangement of straws in the VC.

Table 3
Comparison of CDC and VC characteristics

	CDC	VC
Chamber	Drift chamber	Straw tubes
Layers	4	12
Gas	$Ar/CO_2/CH_4$	Ar/ethane
Pressure	1 atm	3 atm
Beam pipe	2 mm Al	1.2 mm Be

Insulating feedthroughs are held in each end of a straw by aluminum inserts glued to the straws with conductive epoxy. The feedthroughs are fixed to the inner precision endplates by aluminum nuts, holding the straws in tension between these endplates. Slots in the feedthroughs allow gas to pass through them into the straws.

The chamber is designed to hold a gas pressure of 5 atm. But it is operated at 3 atm. The working gas is argon/ethane (50%/50%) and the design voltage is 3.7 kV. The inherent single-hit resolution of the VC is about 50 μm. However, since BESII uses TDCs with 2 ns bins (equivalent to about 50 μm of electron drift) the final single-hit resolution is 73.4 ± 8.4 μm from cosmic rays and 90 μm from colliding beam data. Table 3 shows the comparison of the VC and CDC characteristics.

5. Luminosity monitor (LUM)

The BES luminosity monitor provides instantaneous accelerator luminosity online and allows for offline calculation of integrated luminosity. With the upgrade of BEPC came the requirement to replace the first BES luminosity monitor (LUMI) [8], because it was displaced by new final focus quadrupoles. The new luminosity monitor (LUMII) has to satisfy severe space constraints, and its read-out must function in a magnetic field.

The new luminosity monitor is a four-arm device in the horizontal plane. Each arm consists of a defining counter (P), a coincidence counter (C), and a shower counter (S) to measure the electromagnetic energy. As usual, the goal is to measure the luminosity by measuring the rate of small angle Bhabha scattering. The triggering rate from
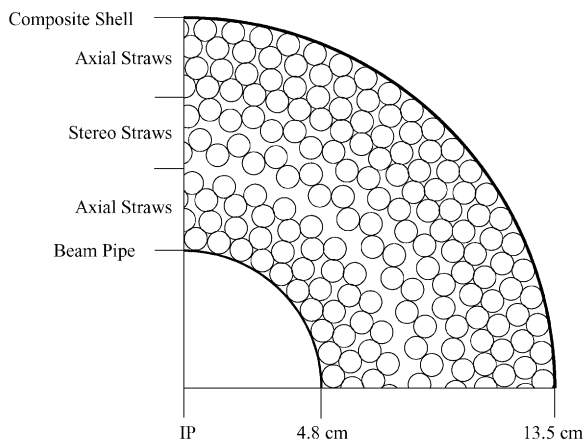

Fig. 2. Quarter section through the vertex chamber. Adjacent layers are paired as superlayers with the straws arranged such that there are no gaps in ϕ in any superlayer. The figure shows straw positions at one endplate.
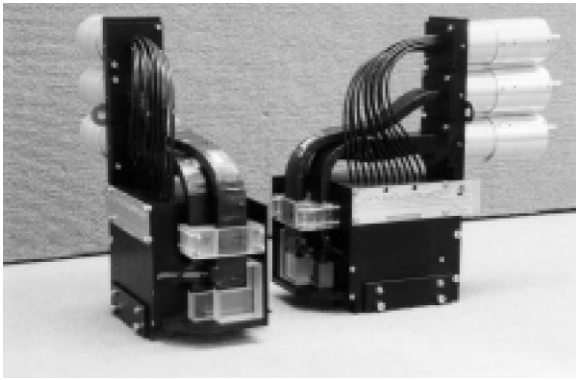
Fig. 3. Two arms of the luminosity monitor.

Bhabha scattering for the proposed luminosity monitor is approximately 10 Hz for a luminosity of 5×10^{30} cm^{-2} s^{-1} at $E_{cm} = 4$ GeV. Fig. 3 is a photograph of the luminosity monitor.

Because of the space constraints, tungsten (95% by weight) is used as the radiator in the shower counter. This counter is a 12-layer device, with each layer consisting of a 3.5 mm sheet of tungsten followed by a 4 mm sheet of plastic scintillator. Thus, the total length of the shower counter is approximately 12 radiation lengths. The tungsten plates are slightly larger than the interleaved scintillator, and are held in place by grooves in the top and bottom of the enclosure. The scintillator is SCSN-81. The mass of tungsten in each arm is 7 kg. The defining counters are 8 mm thick, and rectangular in shape, with dimensions of 28×40 mm^2. The minimum angle accepted is 64 mrad.

The coincidence counters must be large enough to have full acceptance for a Bhabha scattering which intersects the opposite P counter, considering the finite bunch length. This results in a rectangular counter of dimensions 50×54 mm^2, again chosen to be 8 mm thick. All counters are viewed by Hamamatsu 1.5 in. R5946 fine-mesh photomultipliers, which will function in the 0.4 T magnetic field of BES.

Most of the luminosity monitor electronics from LUMI have simply been reused. The PMTs are connected, after suitable delay lines, to the discriminator (LeCroy 623B and Phillips 715) and ADC (LeCroy 2249A) electronics via LeCroy 428F linear fan-in/fan-out modules.

The trigger is of the form $(P_i S_i) \cdot (C_j S_j)$, where i and j refer to counters in opposite directions from the IP. To aid in subtracting backgrounds, there is a corresponding trigger with $(C_j S_j)$ delayed by one beam crossing (800 ns). There is also a pre-scaled beam-cross trigger, which is variable, but typically set at one in 10^6 beam crossings in the present implementation.

For diagnostic purposes and to monitor stability, there is a pulsing system to pulse LEDs which shine on the scintillator. This system is able to pulse-single counters, and also pulse counters according to the trigger requirements.

All counters, P, C and S, were tested with cosmic rays and with LED pulses prior to installation. The results are in good agreement with calculations based on our experience and Monte Carlo simulation. We have observed ~ 50 pe, ~ 90 pe and ~ 40 pe in P, C, and S counters, respectively. Our Monte Carlo simulation indicates that a typical BES Bhabha event (2 GeV/c electron or positron) deposits about 100 MeV in the S counter (~ 100 times more than a minimum ionization cosmic ray muon does), and therefore leads to a signal of ~ 4000 pe. The timing resolution of the P & C counters is measured to be ~ 0.3 ns which is sufficient to distinguish Bhabha events from beam-gas events (0 vs. 8 ns).

Under running conditions at the J/ψ the observed resolution of a shower counter on Bhabha electrons is 23%. This is significantly larger than the predicted value of 16% from simulations. The difference is not yet understood, but possible contributions include inaccuracies in the simulation, e.g., in the modeling of the material preceding the shower counter, or in noise from machine backgrounds.

6. Trigger system

The BES trigger consists of three decision levels. The first-level trigger is produced in one collision period (0.8 μs), while the second and third levels take four collision periods. The trigger logic uses information from the TOFII, SC, MDCII, VC, and muon counters. Because the VC replaced the CDC and because MDCII has significantly different

characteristics than MDCI, new trigger systems for the VC and the MDCII were constructed.

The MDCII trigger uses signals from the non-stereo layers, 2, 4, 6, and 8, to find charged track candidates in the (r,ϕ) plane. First, cell hits are found requiring signals on at least three out of the four sense wires in a drift cell. The positions of the hit cells are then used to find potential track candidates using combinations of cells in the four layers. Possible layer combinations for constructing tracks are layers 2, 4, and 6; 2, 6, and 8; or 2, 4, and 8. Track candidates must pass through the interaction point and have a radius of curvature greater than 83.3 cm, corresponding to a momentum greater than 100 MeV in a magnetic field of 0.4 T. A good track is the "OR" of the three possible layer combinations. The total possible number of combinations for good tracks in $\frac{1}{8}$ of the MDC is 287.

Fig. 4 shows the diagram of the MDCII logic. A total of 1152 pairs of ECL differential signals from MDCII are converted to TTL and processed by the "3 out of 4" logic to find cell hits. Tracks are constructed from the hit cells using the Track Finding module. The Track Counting module outputs signals to the secondary level trigger corresponding to ≥ 1, ≥ 2, or ≥ 4 tracks. A veto module may be used to suppress events with too many tracks. Back-ground events may also be suppressed by using the matching circuit. This logic matches tracks found in MDCII with hits in the VC and TOF systems.

Fig. 5 shows the logic diagram of the VC trigger. The four innermost and four outermost layers (the axial layers) are used for trigger decisions. Adjacent layers (1 and 2, 3 and 4, etc.) are combined to form superlayers. Straws hit in either of these layers make superlayer hits. Hits in either of the inner two superlayers are then matched with hits in either of the outer two super layers to form track candidates. Because the tracking thickness of the VC is only 13 cm, tracks in this detector can be considered to be straight lines.

7. Data acquisition and computing

Deadtime in the DAQI system of BESI was around 20 ms per event. With the increase in the luminosity of BEPC by a factor of two or three, this dead-time would result in an unacceptable loss of data. Thus, the goal of upgrading DAQI was to reduce the deadtime to 10 ms per event.

In contrast with DAQI, which was centralized on a VAX-785, the new DAQII divides the data acquisition task between a DEC Alpha 3600 host for background processes (e.g. detector status, monitoring event rate, event selection, etc.) and a front-end VME subsystem for data acquisition. The systems communicate via Ethernet using
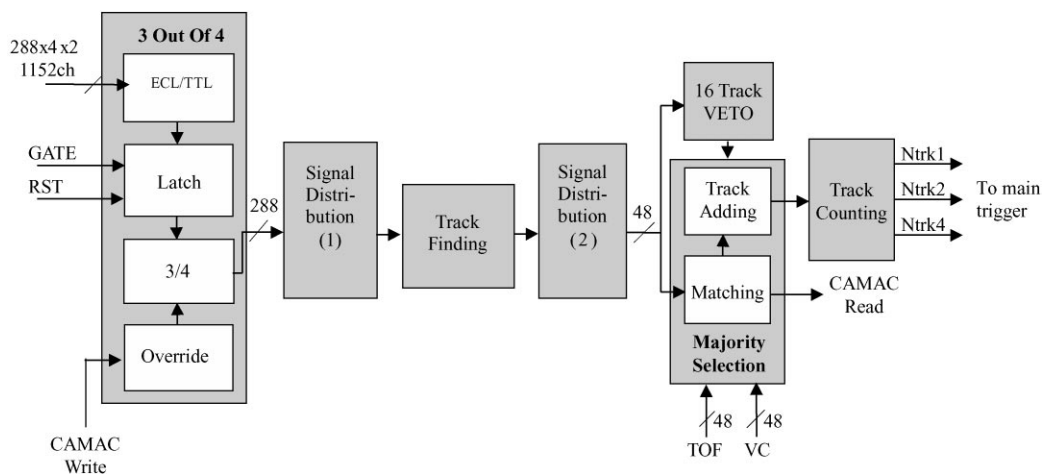

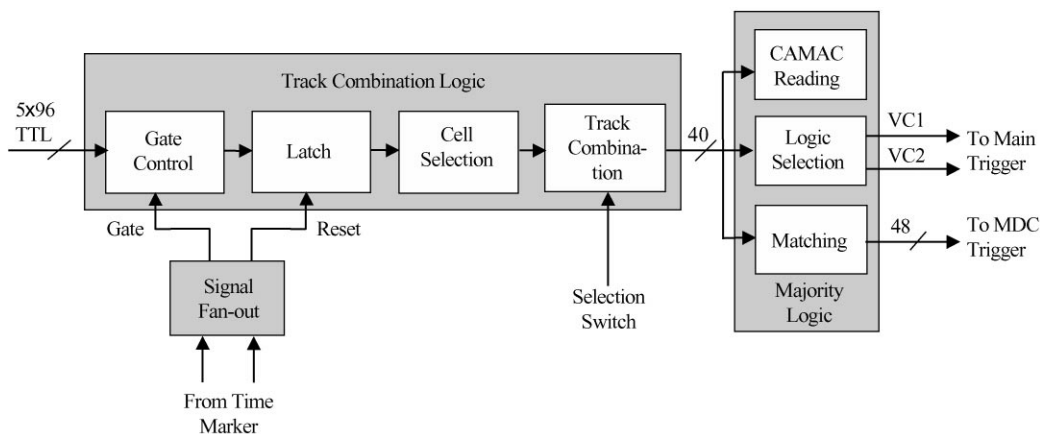Fig. 4. Logic diagram of the MDCII trigger.
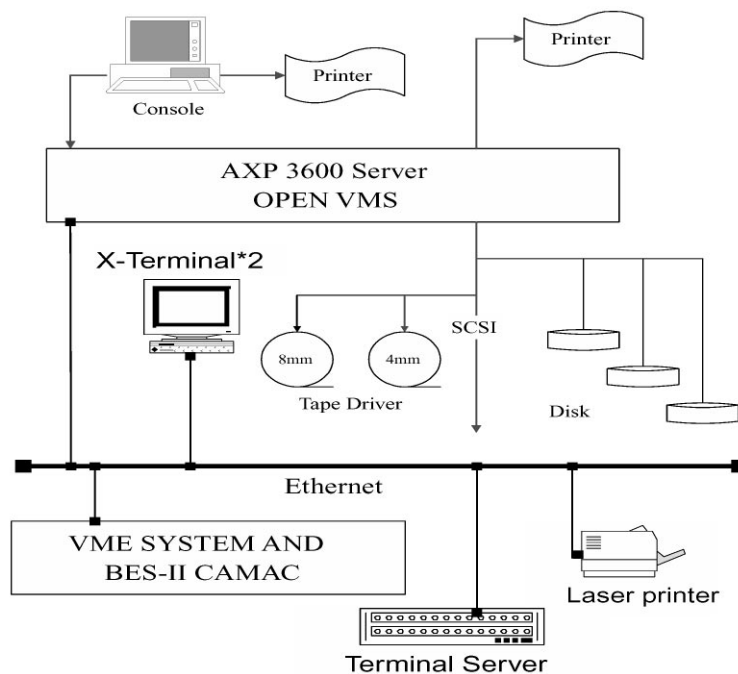
Fig. 5. Logic diagram of the VC trigger.

Fig. 6. Configuration of the host Alpha 3600.

TCP/IP protocol. Fig. 6 shows the configuration of the DAQ system. Table 4 summarizes the comparison between DAQ I and DAQ II.

The front-end data acquisition subsystem consists of CAMAC plus VME and FASTBUS components (Fig. 7). Two MVME162 single board computers execute data acquisition and logging tasks. The CAMAC modules are interfaced to the VME bus via a CAMAC Branch Driver (VCBD).

The electronics of the vertex chamber consist of LeCroy 1879 TDCs and a LeCroy 1821 FASTBUS Segment Manager/Interface Module. The LeCroy 1821 is linked to the VME via a LeCroy 1131

Table 4
Comparison of DAQI and DAQII characteristics

	DAQI	DAQII
CPU	VAX785	Alpha3600
Interface	VAX–VCC–CAMAC	VME–VCBD–CAMAC
BADC	21	29
Mode	Series	Parallel
Time/event	20 ms	10 ms

VME-to-SIB (standard interface bus) interface module. To reduce ADC conversion time, the number of BADCs was increased from 23 to 31 in BESII.

The increase in the amount of data due to the increased luminosity of BEPC required increasing the offline computing power. This was accomplished by replacing the aging VAX/VMS system with HP/UNIX machines. Offline analysis software was upgraded to include VC tracking, fitting, and track matching with MDCII. In addition, a new GEANT based simulation package has been developed. The BES software library is managed by the Codeman system on UNIX platforms located at different BES sites.

A new algorithm using a non-numerical pattern recognition technique, first developed by the MAR-KIII collaboration [9], is used for finding MDC and VC tracks [10,11].

8. Performance of BESII

A summary of the performance of BESII is shown in Table 5. These results were obtained from an analysis of 2 million J/ψ events.

The VC has 95% hit efficiency and low noise at an operating voltage of 3700 V. Fig. 8 shows the tracking residuals in the VC compared to the CDC. Position resolution in the VC has reached 90 μm.

With the split voltage scheme implemented in MDCII, noise and leakage current problems have been suppressed. The dark current and noise depend strongly on the temperature of the body of the chamber. The noise level can be limited to that of
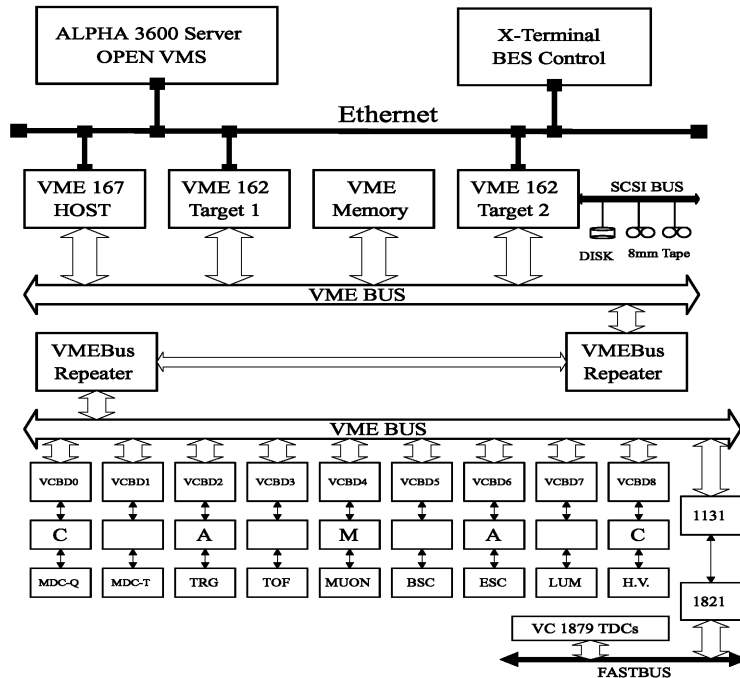

Fig. 7. Diagram of hardware for BESII online system.

Table 5
Performance comparison of BESI and BESII

Subsystem	Variable	BESI	BESII
MDC	$\Delta P/P$	$1.76\%(1 + P^2)^{1/2}$	$1.78\%(1 + P^2)^{1/2}$
	σ_{xy}	200–250 μm	198–224 μm
	$\Delta E/\Delta x$	7.8%	8.0%
VC	σ_{xy}	220 μm	90 μm
TOF	σ_T	375 ps	180 ps
SC	$\Delta E/E$	24.4%	21%
DAQ	Time/event	20 ms	10 ms

Fig. 9. Energy loss resolution in MDCII.
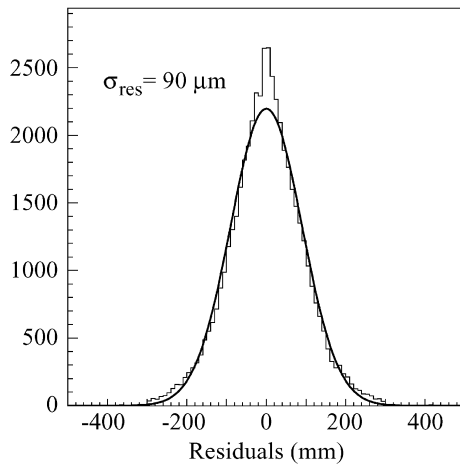
Fig. 8. Single-hit tracking residuals in the vertex chamber.

Fig. 10. Velocity measured by Time-of-Flight counters (TOFII) vs. particle momenta.

BESI by keeping the temperature lower than 25°C. The momentum resolution and dE/dx resolution of MDCII are almost the same as MDCI. Momentum resolution for 1.5 GeV/c Bhabha events has been improved from 50 to 40 MeV/c by combining VC data with MDCII data. Fig. 9 shows the energy loss resolution of MDCII.

Because of the new detector design and a shorter bunch length, TOFII works much better than TOFI. The time resolution is about 180 ps for Bhabha events. Good separation of charged pions, kaons and protons is provided in the momentum region of less than 1 GeV/c (see Fig. 10).

The average readout time of DAQII is less than 10 ms per event, compared to more than 20 ms per event for the DAQI. Data processing, event reconstruction, and physics analysis for an R value measurement from 2 to 5 GeV shows that the up-
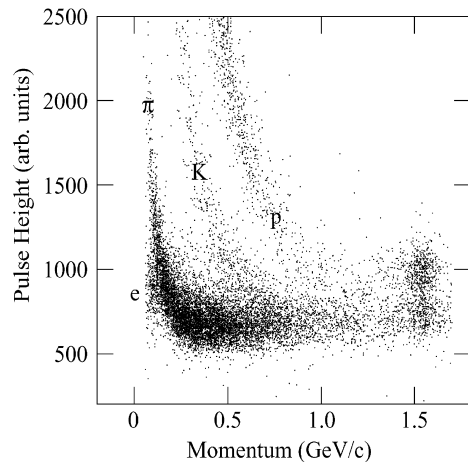
grading of the CPU, network and software have been successful [7].
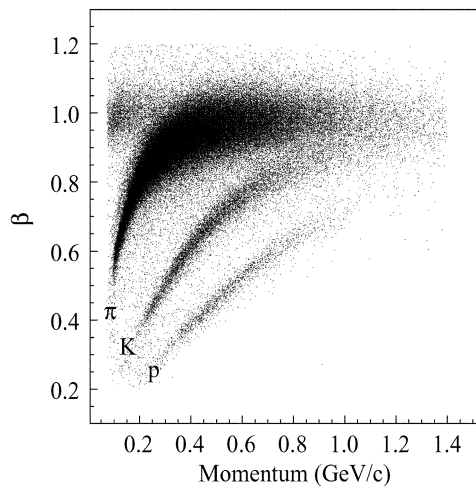
References

[1] J.Z. Bai et al., Nucl. Instr. and Meth. A 344 (1994) 319.
[2] J.Z. Bai et al., Phys. Rev. Lett. 76 (1996) 3502.
[3] J.Z. Bai et al., Phys. Rev. Lett. 81 (1998) 3091.
[4] J.Z. Bai et al., Phys. Rev. D 52 (1995) 3781.
[5] J.Z. Bai et al., Phys. Rev. D 53 (1996) 20.
[6] Y. Wu, Operational status and future upgrades of the BEPC, Talk given at the 18th Particle Accelerator Conference, New York, March 1999.
[7] J.Z. Bai et al., Phys. Rev. Lett. 84 (2000) 594.
[8] H. Ni et al., High Energy Phys. Nucl. Phys. 14 (1989) 238.
[9] J.J. Becker et al., Nucl. Instr. and Meth. A 235 (1985) 502.
[10] J. Liu et al., High Energy Phys. Nucl. Phys. 22 (1998) 587.
[11] G.P. Chen et al., High Energy Phys. Nucl. Phys. 22 (1998) 982.